Inversion of First Kind Volterra Equations: Back to Direct Methods?

Luis E. Bilbao [1] and Diana E. Grondona [2]

Instituto de Física del Plasma, INFIP-CONICET, Facultad de Ciencias Exactas y Naturales, Universidad de Buenos Aires, Ciudad Universitaria, Pab. I, 1428 Buenos Aires, Argentina

Z. Naturforsch. **48a**, 1119–1130 (1993); received June 25, 1993

Numerical inversion of the first kind Volterra equation (the Abel inversion included) has been extensively studied. Direct methods were probably the first methods used to attempt the inversion. Together with the computer hardware evolution, new methods were devised in order to deal with the inherent problem of this kind of equation, that is, error magnification. Using a large number of data points (several thousands) most methods are difficult to use, specially when the inversion and its error are required on line, that is, while performing the experiments. Further, error propagation (coming from the input data and from the parameters of the problem) is, usually, a difficult task and has not been extensively studied. On the other hand, direct methods together with an adequate filter give good resolution, are fast, and error propagation is easily performed. In this work we used the so called Matrix Method for inverting three different equations, showing how to build the resolvent nucleus and how errors propagate through the solution.

Key words: First kind Volterra equations; Abel equation; Direct method; Matrix method; Error propagation.

1. Introduction

Volterra equations are found in many problems in Physics. In particular, in Plasma Focus (PF) research [1] we deal with three different equations:

a) The plasma density measured from interferometry [2, 3], assuming cylindrical geometry, for an Nd laser (530 nm) is obtained as

$$S(x) = 2.37 \times 10^{-22} \int_x^R \mathrm{d}r\, n(r) \frac{2r}{\sqrt{r^2 - x^2}}, \qquad (1)$$

where $S(x)$ is the fringe displacement, $n(r)$ the plasma density as a function of the radius, and R the radius of the column (MKS units are used, except where noted). This is the well known Abel integral. Defining

$$s(x) = 2.11 \times 10^{21}\, S(x) \qquad (2)$$

and

$$L(r, x) = \frac{r}{\sqrt{r^2 - x^2}}, \qquad (3)$$

a scaled form of (1) is obtained as

$$s(x) = \int_x^R \mathrm{d}r\, n(r)\, L(r, x). \qquad (4)$$

The kernel $L(r, x)$ is plotted in Fig. 1 for $R = 1$ and different values of x.

b) The magnetic signal sensed by a probe is a convolution between the actual current density, j, and the perturbation introduced by the probe body [4]. For a spherical tip of a cyclindrical probe of radius a, the perturbed magnetic field is [4]

$$B(z-d) = \mu_0 \int_0^z \mathrm{d}z'\, j(z')\, M\left(\frac{z - z' - d}{r(z - z')}\right), \qquad (5)$$

where z is the position of the probe tip ($z-d$ is the location of the sensing coil), $M(\zeta)$ the Malberg function [5], d the distance from the coil to the probe tip and r the radius of the probe

$$r(\eta) = \begin{cases} a & \eta \geq a, \\ \sqrt{a^2 - (\eta - a)^2} & 0 < \eta < a, \\ 0 & \eta \leq 0. \end{cases}$$

Actually, the voltage measured by the probe is proportional to the time derivative of the magnetic flux

$$V(t) = \frac{\mathrm{d}\phi}{\mathrm{d}t}, \qquad (7)$$

[1] Member of the Carrera del Investigador, CONICET, Argentina.
[2] Fellow of CONICET, Argentina.

Reprint requests to Prof. Dr. L. Bilbao, Instituto de Física del Plasma, Ciudad Universitaria, Pab. I, 1428 Buenos Aires, Argentina.

0932-0784 / 93 / 1100-1119 $ 01.30/0. – Please order a reprint rather than making your own copy.

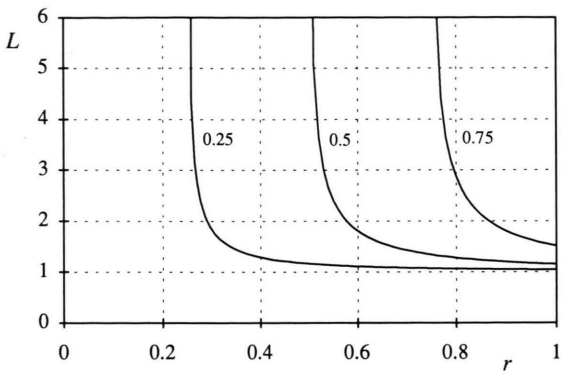

Fig. 1. Kernel for the Abel inversion for $R=1$ and $x=0.25$, 0.5, 0.75.

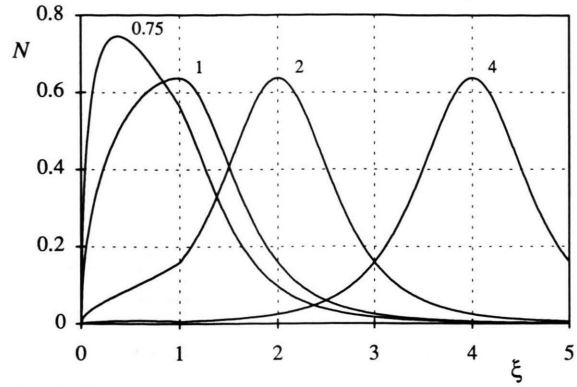

Fig. 2. Kernel for the magnetic probe problem for $a=1$ and $d=0.75$, 1, 2, 4.

where the flux can be approximated, as long as the radius of the coil is much smaller than the radius of the probe, by

$$\phi = AB\,, \tag{8}$$

A being the area of the coil. Further, assuming that the current distribution propagates at a constant speed U, therefore

$$z = U\,t \tag{9}$$

and the measured voltage, (7), becomes

$$V(t) = \mu_0 UA\, j(z+d)\, M\left(\frac{-d}{r(0)}\right) + \mu_0 UA \int_0^z \mathrm{d}z'\, j(z')\, \frac{\partial M}{\partial z}\left(\frac{z-z'-d}{r(z-z')}\right). \tag{10}$$

Using the fact that the first term on the right hand side of (10) is zero, because $M(-\infty)=0$, we get

$$V(t) = \mu_0 UA \int_0^z \mathrm{d}z'\, j(z')\, \frac{\partial M}{\partial z}\left(\frac{z-z'-d}{r(z-z')}\right). \tag{11}$$

Calling

$$v(z) = \frac{V(t)}{\mu_0 UA} \tag{12}$$

and

$$N(\xi) = \frac{\partial M}{\partial \xi}\left(\frac{\xi - d}{r(\xi)}\right), \tag{13}$$

then (11) becomes

$$v(z) = \int_{-0}^{z} \mathrm{d}z'\, j(z')\, N(z-z')\,. \tag{14}$$

The kernel N is plotted in Fig. 2 for $a=1$ and different values of d.

Note that the kernel vanishes for $\xi=0$. The fact $N(0)=0$ gives to the integral equation (14) some particular properties, similar to the case of a linear differential equation when the coefficient of highest order is zero. The way to overcome the problem is deriving (14): A second kind Volterra equation is obtained, as long as the first derivative of $N(0)$ is not. This condition is fulfilled when $d/a<1$. For larger values of d/a the first derivative becomes smaller and the singularity becomes more serious. To avoid this, we construct the probes locating the coil at a distance shorter than the radius of the coil.

c) Using a calibrated photo-detector, it is possible to obtain the plasma density from the light intensity emitted by the plasma. The measured voltage, $W(x)$, generated by the photo-detector, is [6]

$$W(x) = \frac{2K}{\sin\phi} \int_0^x \mathrm{d}x'\, n^2(x')\, \frac{[1+G(x-x')]}{\sqrt{[1+G(x-x')]^2-1}}\,, \tag{15}$$

where K is a dimensional constant containing the sensibility and characteristics of the photo-detector plus the optical system, ϕ is the angle between the plasma and the axis of symmetry, n the plasma density, x a coordinate perpendicular to the plasma and G a geometrical factor,

$$G = \frac{1}{r_0 \sin\phi}\,, \tag{16}$$

r_0 being the radial position at which the emitted light is observed. Using

$$w(x) = \frac{W(x)}{2K r_0} \tag{17}$$

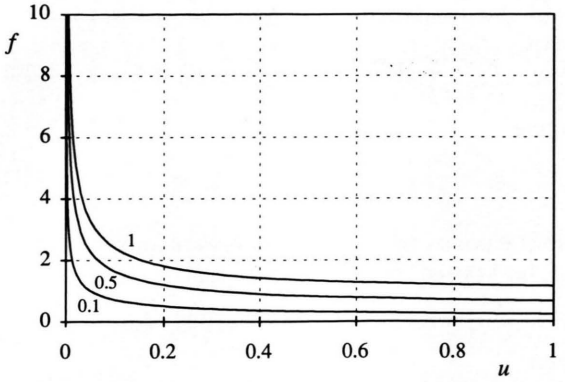

Fig. 3. Kernel for the photodetector problem for $G=0.1$, 0.5, 1.

and

$$f(u)=\frac{G(1+Gu)}{\sqrt{(1+Gu)^2-1}}. \tag{18}$$

Equation (15) becomes

$$w(x)=\int_0^x \mathrm{d}x'\, n^2(x')\, f(x-x'). \tag{19}$$

The kernel $f(u)$ is plotted in Fig. 3 for different values of the parameter G.

All three cases, (4), (14) and (19) are first kind Volterra equations; cases b) and c) are called convolution equations because the difference $z-z'$ or $x-x'$, respectively, appears in the kernel.

2. Requirements for the Inversion Procedure

There are numerous methods for solving Volterra equations when the input function is continuous, for example using the Laplace transform. The experimental data are discrete in nature, and a numerical inversion is needed. Further, the experimental data have some error, and it is not clear *a priori* how this error affects the solution and/or the numerical procedure.

Volterra equations (in particular, the Abel integral) have been extensively studied [7]. It is well known that first kind Volterra equations are a not well-posed problem in the sense of Hadamard [8]. This is due to the fact that a small change in the measured value, the left hand side term in (4), (14), and (19), produces a large change in the unknown function. This is inherent to the problem and does not depend on the numerical method. It can be explained as follows. Considering a plateau followed by another plateau one step up, and recalling that the measured data are the *integral* of the unknown function, the step in the integral is interpreted as a positive peak in the unknown distribution (a delta function when the spacing goes to zero), followed by a negative peak to keep the integral constant in the second plateau. The height of the peak is proportional to the height of the step and to the inverse of the spacing. Although the amplification factor can be very large, the situation is not as serious as it is in an ill-posed problem (like the Fredholm integral equation of the first class [7]), because the magnification error is bounded. This fact requires that for solving first kind Volterra integral equations it is convenient to smooth the input data by means of least squares methods, Fourier approximations, or an adequate filter.

Moreover, as it will be shown in Paragraph 4, the largest magnification factor occurs for short wavelength perturbation. Knowing this, it is reasonable to choose the input data spacing smaller than the minimum physical resolution of the detection system (for example, the spacing several times smaller than the size of the coil in the magnetic problem), and then to filter this wavelength (smaller than the resolution of the system).

For the Abel integral (4), several numerical inversion methods were developed; some of the older ones can be found in [2, 9–11]. In [12] a comparison among different methods is given. Although it is limited to four cases (named as Matrix Method, *h*-interpolation, *f*-interpolation, and Fourier Method – the Convolution method is not used for radial symmetrical objects –) it represents the main ideas for solving the Abel equation. The Matrix Method is a direct method while the others are different ways to interpolate (smooth) the data, and then to solve for the interpolated function.

Our PF experimental conditions require some extra conditions on the inversion besides those stated in [12]; some of those are:

1) The inversion should be capable of inverting signals recorded at a large number of points, that is, ranging from several hundreds to a few thousands (usually a digitizer is used having more than one thousand data points).

2) It should be possible to calculate the error of the solution from the error of the input data.

3) Because the input data are smoothed (explicitly or implicitly) in order to avoid large oscillations in the solution, the amplification matrix should be given in

order to know whether or not a given wavelength is spuriously included in (or removed from) the results.

4) Usually the inversion is needed *on line*, that is while performing the measurements. This fact requires a fast algorithm.

Among the methods described in [12], the Matrix Method is the only one that permits a simple error propagation from the errors in the parameters and in the input data, and the amplification matrix is easily calculated. Note that some estimation of the error propagation is given in [12] by adding a random error to the test profile. Although this procedure gives some idea of the inversion accuracy (see Fig. 3.13 of [12]), it does not represent the error in the inverted signal. For example, there are several points where the error crosses the abscissa. It is clear that the error is different from zero for all values of r, therefore, at those points, how large the error is? Following this procedure, the way to simulate the statistical error is to repeat several times the inversion (one thousand times, say) with a randomly generated error, and then, to calculate the dispersion of the output data. Of course this procedure requires a large amount of computer time. Nevertheless, using the Matrix Method it is possible to give an expression for the inverse of the kernel (a fact that has not been widely used) and to propagate errors, as it is shown below.

3. The Matrix Method

Direct methods perform quite well for solving first kind Volterra equations [7]. In particular, for (14) it seems to be the only way to calculate the numerical inversion, due to the singularity of the kernel shown in Paragraph 1. The Matrix Method of [12] is closely related to the Midpoint Method of [7], as long as the inverted values of the Matrix Method are assigned to the center of the interval (and not to the one of the boundaries, as stated in [12]). Both are $O(\Delta x^2)$ approximations which can have non negligible errors when few (less than 50, say) points are used. Today, acquisition systems (digitizers, CCD cameras) work with thousands of points, making this error negligible as compared with the experimental errors in the detection of the signals.

In what follows, we will use an equally spaced grid. The Matrix method does not depend on this hypothesis, however the error propagation analysis is greatly reduced in this limit.

a) The discrete form of (4) can be written as

$$s_i = \sum_{j=1}^{N-1} \int_{x_j}^{x_{j+1}} \mathrm{d}r\, n(r)\, L(r, x_i), \quad 0 \le i \le N-1, \tag{20}$$

where

$$x_i = \frac{iR}{N}, \quad 0 \le i \le N \tag{21}$$

are the points where the values s_i are known.

The Matrix Method assumes that

$$n(r) = n_{j+\frac{1}{2}}, \quad x_j \le r \le x_{j+1}; \tag{22}$$

then

$$s_i = \sum_{j=i}^{N-1} I_{ij}\, n_{j+\frac{1}{2}}, \quad 0 \le i \le N-1, \tag{23}$$

where

$$I_{ij} = \sqrt{x_{j+1}^2 - x_i^2} - \sqrt{x_j^2 - x_i^2}. \tag{24}$$

In order to simplify the notation, in what follows $n_{j+\frac{1}{2}}$ will be replaced by n_j. In a similar way for the case b) j_k will refer to $j_{k-\frac{1}{2}}$, and in c) n_k^2 will refer to $n_{k-\frac{1}{2}}^2$.

Note that, using a uniform grid, the matrix I can be written as

$$I_{ij} = \Delta x\, I'_{ij}, \tag{25}$$

that is the spatial interval multiplied by a "universal" matrix

$$I'_{ij} = \sqrt{(j+1)^2 - i^2} - \sqrt{j^2 - i^2} \tag{26}$$

that can be calculated and stored in advance in order to speed up the calculation.

It is not necessary to invert the matrix I_{ij} in order to get the solution. A recursive method may be used, giving

$$n_i = \frac{1}{I_{ii}} \left(s_i - \sum_{j=i+1}^{N-1} I_{ij}\, n_j \right), \quad 0 \le i \le N-1. \tag{27}$$

Anyway, in order to study the error propagation, it is convenient to explicitly write down the inverse of the kernel (24) as follows:

$$n_i = \sum_{j=i}^{N-1} B_{ij} s_j, \quad 0 \le i \le N-1. \tag{28}$$

with

$$B_{ii} = \frac{1}{I_{ii}}; \qquad B_{ij} = -\sum_{k=i}^{j-1} B_{ik} \frac{I_{kj}}{I_{jj}}. \tag{29}$$

The inverse of the kernel will be referred as resolvent kernel.

If (26) is used, also the resolvent matrix becomes a product between a constant and a "universal" matrix

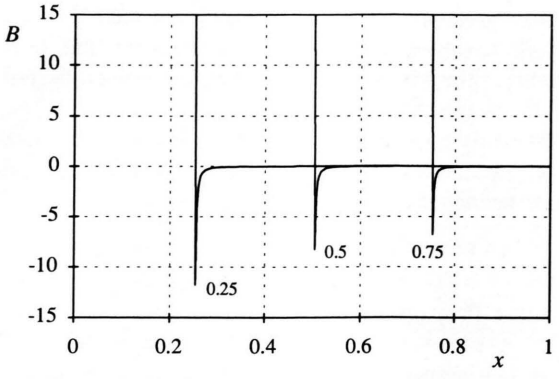

Fig. 4. Resolvent kernel for the Abel inversion for $R=1$, $x_i=0.25$, 0.5, 0.75 and $N=400$.

divided the spatial interval

$$B_{ij}=\frac{B'_{ij}}{\Delta x} \tag{30}$$

with

$$B'_{ii}=\frac{1}{I'_{ii}};\quad B'_{ij}=-\sum_{k=i}^{j-1} B'_{ik}\,\frac{I'_{kj}}{I'_{jj}}. \tag{31}$$

Assuming $N=400$ and $R=1$, the resolvent kernel B_{ij} is plotted in Fig. 4 for $x_i=0.25$, 0.5 and 0.75.

b) For the magnetic probe problem using $z_i=i\Delta z$, (14) becomes

$$v_i=\sum_{k=1}^{i}\int_{z_{k-1}}^{z_k} \mathrm{d}z'\, j(z')\,N(z_i-z') \tag{32}$$

or

$$v_i=\sum_{k=1}^{i} H_{i-k+1}\,j_k \tag{33}$$

with

$$H_{i-k+1}=M\left(\frac{(i-k+1)\,\Delta z-d}{r((i-k+1)\,\Delta z)}\right)-M\left(\frac{(i-k)\,\Delta z-d}{r((i-k)\,\Delta z)}\right). \tag{34}$$

Again, there are two possibilities for solving this equation: a recursion method or inversion of the kernel. This inversion gives

$$j_i=\sum_{k=1}^{i} C_{i-k+1}\,v_k, \tag{35}$$

where

$$C_1=\frac{1}{H_1};\quad C_m=-\sum_{k=1}^{m-1} C_k\,\frac{H_{m-k+1}}{H_1}. \tag{36}$$

In Fig. 5 the resolvent kernel C is plotted for $a=1$ and different values of d. Note the difference with the

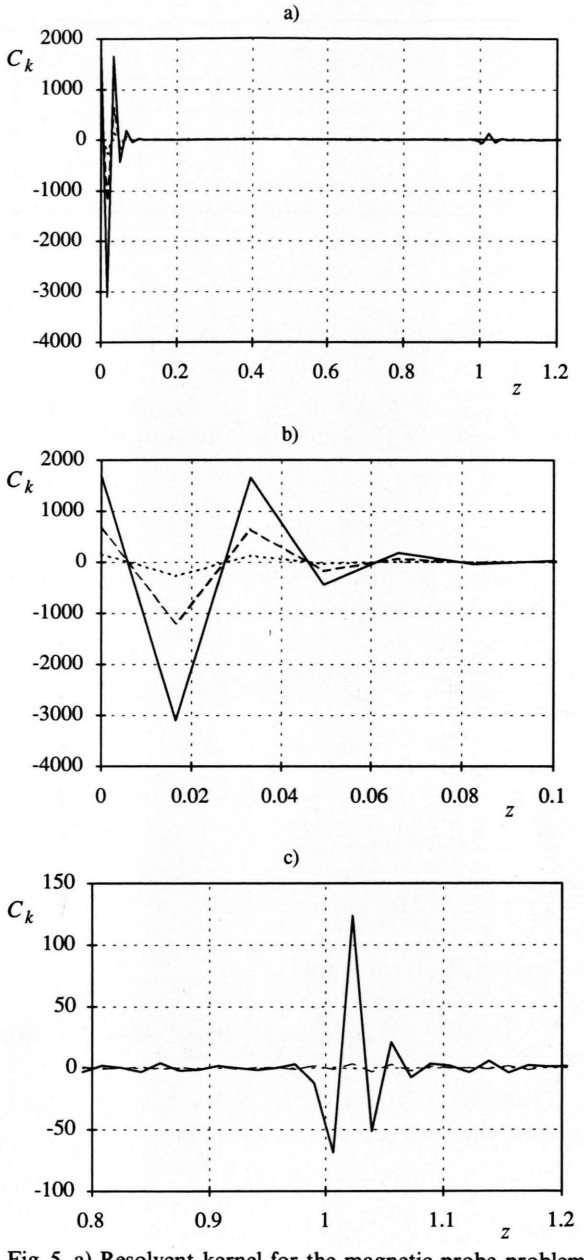

Fig. 5. a) Resolvent kernel for the magnetic probe problem for $a=1$, $N=300$, $\Delta z=1/60$, and different values of d: 2/3 (dotted line), 1 (dashed line), and 4/3 (solid line). b) Magnified view for $z<0.1$. c) Magnified view for $z\approx a=1$.

Abel inverse. The kernel C has a strong $\lambda=2\Delta z$ plus $\lambda\approx a$ oscillations, particularly when $d>a$. This is due to the singularity of the kernel for $z=0$. This kind of kernel produces a large short wavelength amplification, and a filter is mandatory.

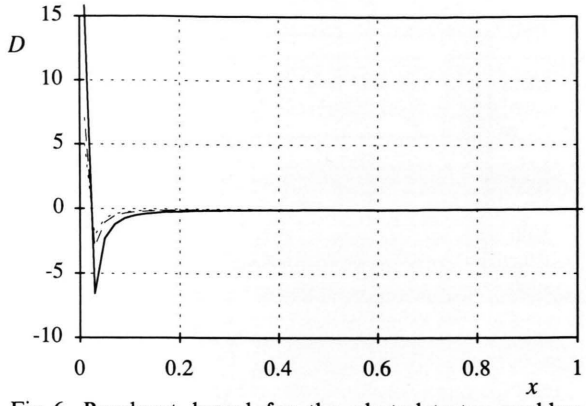

Fig. 6. Resolvent kernel for the photodetector problem, using $N=400$, $\Delta x=0.02$ and $G=0.1$ (dotted), 0.5 (dashed), and 1 (solid).

c) Finally, the discrete form of the photo-detector problem becomes

$$w_i = \sum_{k=1}^{i} J_{i-k+1}\, n_k^2 \tag{37}$$

with

$$J_{i-k+1} = \sqrt{[1+(i-k+1)\,G\Delta x]^2 - 1} - \sqrt{[1+(i-k)\,G\Delta x]^2 - 1}\,. \tag{38}$$

The inversion gives

$$n_i^2 = \sum_{k=1}^{i} D_{i-k+1}\, w_k\,, \tag{39}$$

where the resolvent kernel is

$$D_1 = \frac{1}{J_1}; \quad D_m = -\sum_{k=1}^{m-1} D_k \frac{J_{m-k+1}}{J_1}. \tag{40}$$

In the limit $NG\Delta x \ll 1$ (N is the number of data points), the matrix J can be written as

$$J_{i-k+1} = \sqrt{2G\Delta x}\, J'_{i-k+1}\,, \tag{41}$$

where

$$J'_{i-k+1} = \sqrt{i-k+1} - \sqrt{i-k}\,, \tag{42}$$

that is, again, a "universal matrix" multiplied by a constant factor. Similarly, the resolvent kernel is

$$D_n = \frac{D'_n}{\sqrt{2G\Delta x}} \tag{43}$$

with

$$D'_1 = 1; \quad D'_m = -\sum_{k=1}^{m-1} D'_k\, J'_{m-k+1}\,. \tag{44}$$

In Fig. 6, the kernel D_m is plotted, for $N=400$, $\Delta x=0.02$ and different values of G. Note that D is similar to the Abel resolvent kernel, and quite different for the magnetic probe kernel.

By studying the matrices B, C, and D it is possible to know the spectral response of the kernel and the error propagation.

4. Error Propagation

a) The resolvent kernel B_{ij} only depends on the spatial interval Δx, see (26) and (31). The error in s_j comes from the error in the measured S_j, (2). Therefore, the error in the density can be written as

$$(\delta n_i)^2 = \left(\frac{\partial n_i}{\partial \Delta x}\right)^2 (\delta \Delta x)^2 + \sum_{j=i}^{N-1} \left(\frac{\partial n_i}{\partial S_j}\right)^2 (\delta S_j)^2\,. \tag{45}$$

Assuming that the error in the input data is constant and using (28), we get

$$(\delta n_i)^2 = n_i^2 \left(\frac{\delta \Delta x}{\Delta x}\right)^2 + (\delta s)^2 \sum_{j=i}^{N-1} B_{ij}^2 \tag{46}$$

with

$$\delta s = 2.11 \times 10^{21}\, \delta S\,. \tag{47}$$

The error in the measured data has two different origins: one is due to the presence of noise (electrical or other kind), and the other due to the acquisition system.

There is no general criterion for stating whether or not a signal is noisy. This depends on the particular measurement. If the noise can be recognized, it is possible to reduce it. If not, the method will use it as a part of the signal, and the short wavelength component of the noise will be amplified by the Matrix method, affecting the solution.

On the other hand, if the acquisition system is digital, the Least Significant Bit (LSB) error can be important because it has a strong short wavelength component. In an 8 bits resolution digitizer, the acquired values are *integers* ranging from 0 to 255. The analog to digital conversion produces an error of about 1/512 ($\frac{1}{2}$ LSB) of the range (if set correctly, the range is of the order of the measured data). Notwithstanding it seems a small value, this fact can be the main source of oscillations in the solution because the amplification factor is proportional to number of points. For 1,000 data points the amplified error can be of the same order of magnitude as the inverted signal. Again, a

short wavelength filter is recommended. Of course, a 12 bits resolution digitizer will improve the results. Round off errors are much smaller in most cases and can be neglected.

b) For the magnetic probe problem, the resolvent kernel depends on several parameters: the distances a, d and Δz; the area of the coil, A, and the speed of the current sheet, U. Then, the error in the current density is

$$(\delta j_i)^2 = \left(\frac{\partial j_i}{\partial a}\right)^2 (\delta a)^2 + \left(\frac{\partial j_i}{\partial d}\right)^2 (\delta d)^2 + \left(\frac{\partial j_i}{\partial \Delta z}\right)^2 (\delta \Delta z)^2 + \left(\frac{\partial j_i}{\partial A}\right)^2 (\delta A)^2 + \left(\frac{\partial j_i}{\partial U}\right)^2 (\delta U)^2 + \sum_{k=1}^{i} \left(\frac{\partial j_i}{\partial V_k}\right)^2 (\delta V_k)^2 . \tag{48}$$

Under a similar hypothesis as in case a), the above expression becomes

$$(\delta j_i)^2 = j_i^2 \left[\left(\frac{\delta A}{A}\right)^2 + \left(\frac{\delta U}{U}\right)^2\right] + (\delta v)^2 \sum_{k=1}^{i} C_{i-k+1}^2 + \sum_{p} (\delta p)^2 \left(\sum_{k=1}^{i} v_k \frac{\partial C_{i-k+1}}{\partial p}\right)^2 , \tag{49}$$

where p is any of the parameters a, d, or Δz, and

$$\delta v = \frac{\delta V}{\mu_0 U A} . \tag{50}$$

Note that this is not the error in v_k, it is just the contribution from the error in V_k.

c) For the photo-detector problem

$$(\delta n_i^2)^2 = \left(\frac{\partial n_i^2}{\partial G}\right)^2 (\delta G)^2 + \left(\frac{\partial n_i^2}{\partial \Delta x}\right)^2 (\delta \Delta x)^2 + \left(\frac{\partial n_i^2}{\partial K}\right)^2 (\delta K)^2 + \left(\frac{\partial n_i^2}{\partial r_0}\right)^2 (\delta r_0)^2 + \sum_{k=1}^{i} \left(\frac{\partial n_i^2}{\partial W_k}\right)^2 (\delta W_k)^2 , \tag{51}$$

and finally

$$(\delta n_i^2)^2 = (n_i^2)^2 \left[\left(\frac{\delta K}{K}\right)^2 + \left(\frac{\delta r_0}{r_0}\right)^2\right] + (\delta w)^2 \sum_{k=1}^{i} D_{i-k+1}^2 + [(\Delta x\, \delta G)^2 + (G\, \delta \Delta x)^2] \left(\sum_{k=1}^{i} w_k \frac{\partial D_{i-k+1}}{\partial y}\right)^2 , \tag{52}$$

where $y = G \Delta x$, and

$$\delta w = \frac{\delta W}{2 K r_0} . \tag{53}$$

As can be seen from (46), (49) and (52), there are three different sources of errors: 1) errors coming from scaling factors, 2) errors from the input data, and 3) errors from the parameters of the kernel. For case a) the only parameter (Δx) becomes a scaling factor, therefore there is no contribution 3). All these contributions can be easily calculated during the inversion procedure.

While designing the measurements it is convenient to have (46), (49), and (52) in mind in order to know *a priori* how the solution is sensitive to the parameters and/or the input data.

Contributions 1) are easily understood and no further details will be given.

To compare the importance of contribution 2) among different methods or different positions in a given method, the following dimensionless magnitudes are defined:

$$\varepsilon_i = \begin{cases} \dfrac{1}{B_{ii}} \sqrt{\displaystyle\sum_{j=i}^{N-1} B_{ij}^2} & \text{case a} , \\ \dfrac{1}{C_1} \sqrt{\displaystyle\sum_{k=1}^{i} C_{i-k+1}^2} & \text{case b} , \\ \dfrac{1}{D_1} \sqrt{\displaystyle\sum_{k=1}^{i} D_{i-k+1}^2} & \text{case c} . \end{cases} \tag{54}$$

In all three cases the values of ε_i are almost independent of i, that means that the error in the input values produces a uniform error in the output data. Only the Abel inversion exhibits a small increment of the error in the axis of symmetry, about 5% larger than the error in the outer part of the column. In Table 1 the mean values of ε_i (among all data points) and their dispersion are given for the parameters used in Figs. 4, 5 and 6. Note that the kernel of case b) propagates the error twice as much as the other cases. This is due to the singularity in $z=0$ that is reflected in the oscillating character of C_k. The main source of this error comes from short wavelength perturbations, as it can be seen defining

$$\chi_m(\lambda) = \frac{1}{C_1} \sum_{k=1}^{i} C_{i-k+1} \cos\left(\frac{2\pi(k-1)\,\Delta z}{\lambda}\right), \tag{55}$$

where λ is the wavelength of the perturbation. In Fig. 7 the values of χ_m are plotted for different values of λ, showing that the component $\lambda = 2\Delta z$ is that of larger magnification. Fortunately, usually this short wavelength is physically meaningless, and a filter can be used to removed it. An explicit filter, of the form

$$\tilde{j}_i = 0.25\,(j_{i+1} + 2 j_i + j_{i-1}) , \tag{56}$$

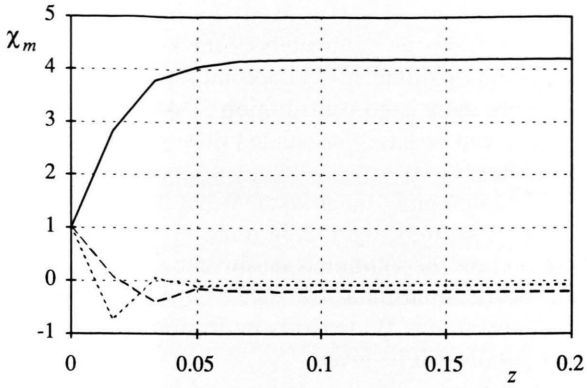

Fig. 7. Error magnification χ as a function of z for $\lambda = 2\Delta z$ (solid), $6\Delta z$ (dashed), and $20\Delta z$ (dotted). The parameters of the kernel are $a=1$, $d=1$, $N=300$, $\Delta z = 1/60$.

Table 1. Mean values of ε and their dispersion for the three different cases.

Case	Parameters	ε
a	$R=1$, $N=400$	1.0990 ± 0.0082
b	$a=1$, $d=2/3$, $\Delta z=1/60$, $N=300$	2.2259 ± 2E-05
b	$a=1$, $d=1$, $\Delta z=1/60$, $N=300$	2.3095 ± 2E-05
b	$a=1$, $d=4/3$, $\Delta z=1/60$, $N=300$	2.3275 ± 0.0004
c	$G=0.1$, $\Delta x=1/50$, $N=400$	1.0976 ± 0.0002
c	$G=0.5$, $\Delta x=1/50$, $N=400$	1.0992 ± 0.0002
c	$G=1$, $\Delta x=1/50$, $N=400$	1.1011 ± 0.0002

removes $\lambda = 2\Delta z$ from the solution (for other filters see, for example, [13]).

Note that, due to the linearity of (28), (35), and (39), filtering the input data is equivalent to either filtering the output data or filtering the resolvent kernel B, C or D, respectively. Therefore, if a filter is used, the filtered kernel must be used in (46), (49) or (52) in order to get the appropriated error propagation.

Finally, for the contribution 3), in order to compare different contributions we define

$$\Delta_p C_m = C_m(p + \tfrac{1}{2}\delta p) - C_m(p - \tfrac{1}{2}\delta p) \approx \delta p \frac{\partial C_m}{\partial p}. \quad (57)$$

In Fig. 8 we plot $\Delta_p C_m$, assuming a 10% error in the parameters a, d, and Δz. The contributions of δa and $\delta \Delta z$ are of the same order while that coming from δd is larger by a factor 2. Then, a more accurate measurement of d is required. From Fig. 8c the influence of the $\lambda \approx a$ perturbation is clear.

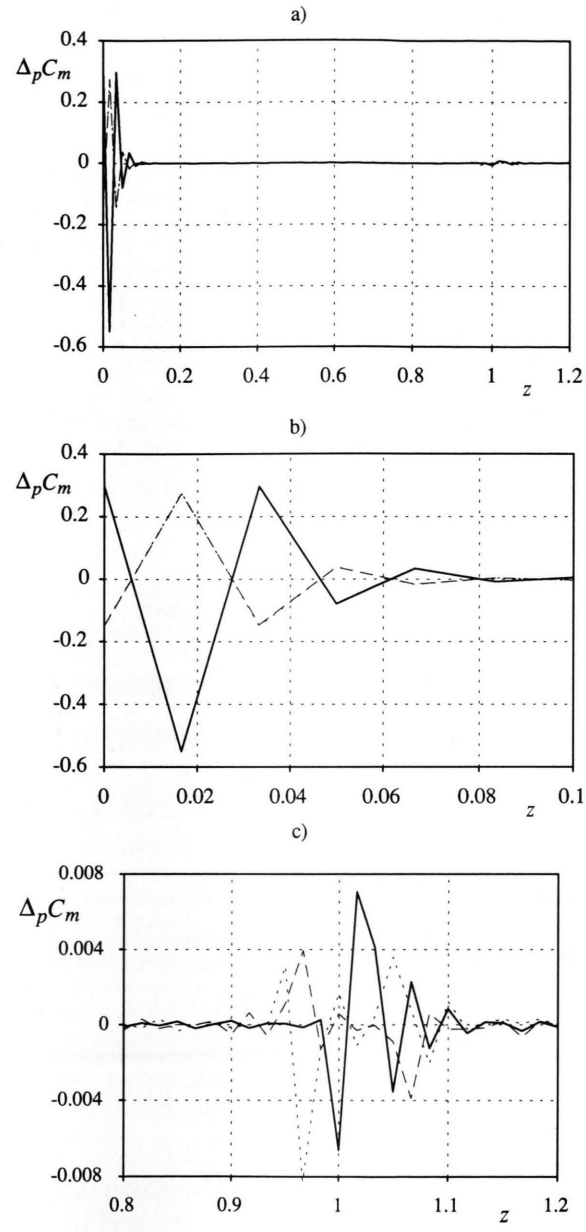

Fig. 8. Magnetic probe problem with $a=1$, $d=1$, $N=300$, $\Delta z = 1/60$. a) Contribution of the parameters to the error, assuming a relative error of 10% for all the parameters: a (dotted), d (solid), and Δz (dashed). b) Magnified view for $z < 0.1$. c) Magnified view for $z \approx a = 1$.

5. Examples

Several test profiles showed that the error in the method is negligible when the parameters are measured with a few percent errors. In all cases, short

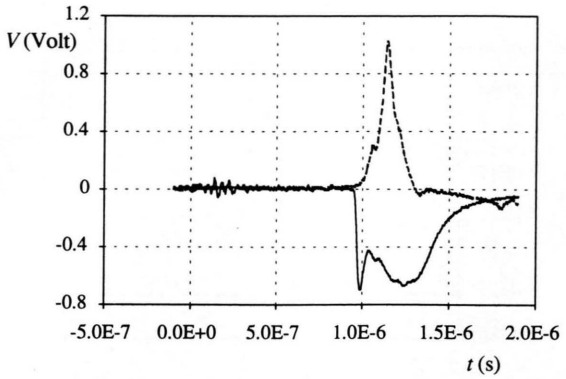

Fig. 9. Measured signals from a magnetic probe – attenuated by 20 – (dashed line) and from a photodiode (solid line) in a Plasma Focus discharge. There is a 50 mV noise at the beginning of the discharge, decreasing under the LBS error in the rest of the signal.

wavelength perturbations are magnified, specially in the case b). An explicit filter worked well in all cases.

In Fig. 9 the measured signals from a magnetic probe (attenuated by 20) and from a photodiode are given, obtained at 0.5 MSample with 1,000 data points.

The parameters are: $A = 10\ \text{mm}^2\ (\pm 5\%)$, $a = 3.5\ \text{mm}$ $(\pm 10\%)$, $d = 3\ \text{mm}$ $(\pm 4\%)$, $r_0 = 27.5\ \text{mm}$ $(\pm 1\%)$, $\sin\phi = 0.743\ (\pm 2\%)$, $K = 1.11 \times 10^{-41}\ \text{Vm}^5\ (\pm 15\%)$ and $U = 5.7 \times 10^4\ \text{m/s}\ (\pm 2\%)$. The errors in the measured voltages due to the analog to digital conversion were 10 mV for the probe (20×) and 8 mV for the photodiode. Note that the radius a is not just the diameter of the probe but the effective radius of the hole produced in the CS, that is expected to be larger than a, as discussed in [4]. This fact was considered as an additional error in a. The actual radius a was measured with 2% error.

There is some significant noise at the beginning of the discharge (see Fig. 9), having 40 ns period, with decreasing amplitude when approaching to the main peak. This noise was not removed for performing the inversion because for this particular wavelength no error magnification is expected.

The inversion of the photodiode is plotted in Fig. 10a. As was expected, the oscillations at the beginning of the discharge do not propagate through the inversion and decrease as the noise decreases in the input data. Although a filter was used, the short wave amplification is evident. Anyway, these perturbations remain bounded. An enlarged view of the peak of the inversion is shown in Fig. 10b, while error contribu-

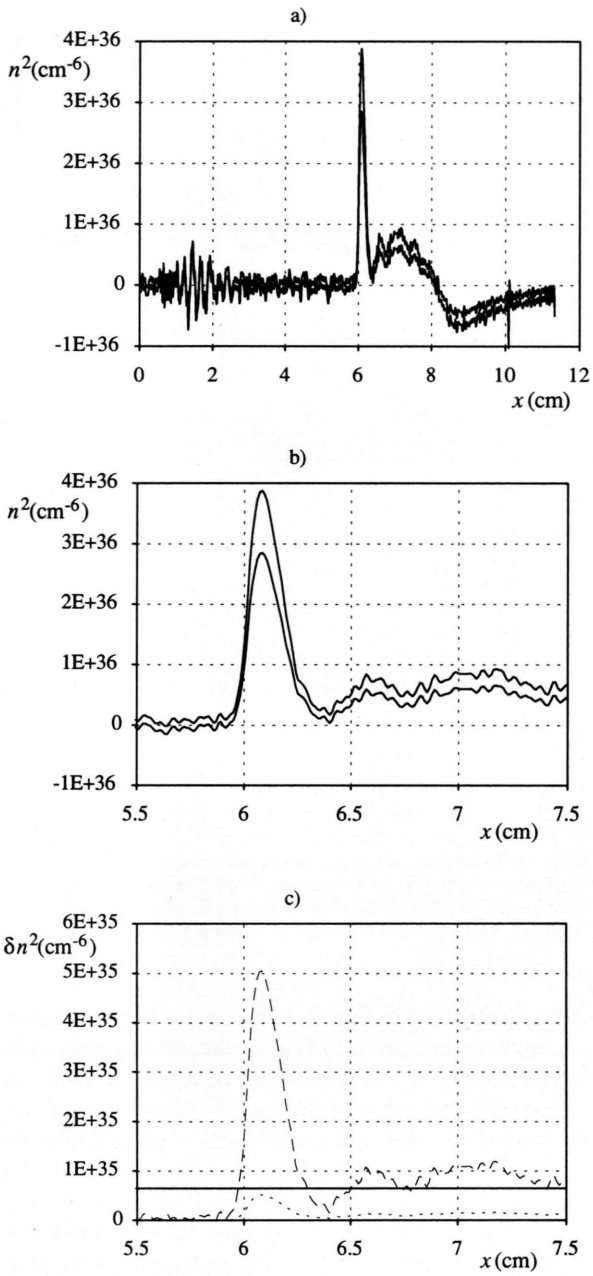

Fig. 10. Inversion of the photodiode signal and the associated error band. a) Inversion from the beginning of the discharge. b) Magnified view of the main peak of the density. c) Error contributions: scaling factors – contribution 1) – (dashed), error in the input data ($\frac{1}{2}$ LSB) – contribution 2) – (solid), and parameters of the kernel – contribution 3) – (dotted).

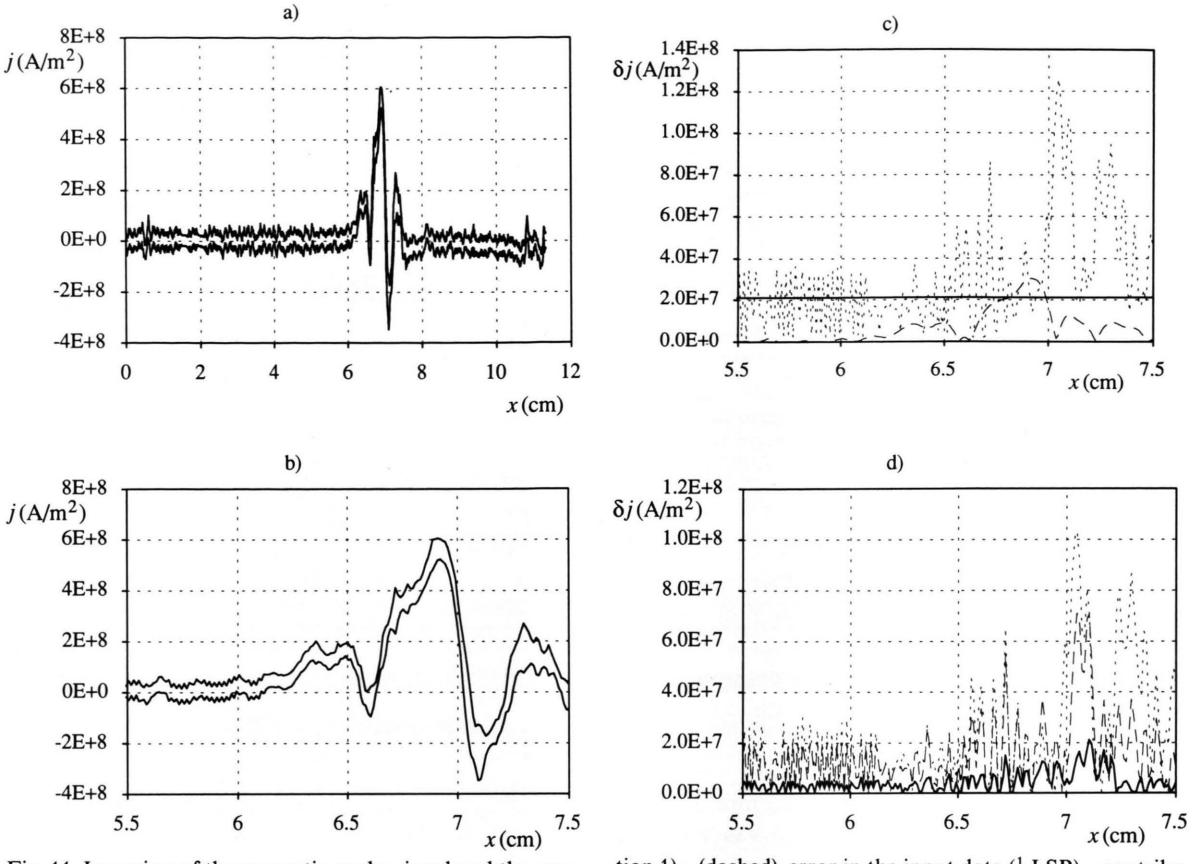

Fig. 11. Inversion of the magnetic probe signal and the associated error band. a) Inversion from the beginning of the discharge. b) Magnified view of the main peak of the current density. c) Error contributions: scaling factors – contribution 1) – (dashed), error in the input data ($\frac{1}{2}$ LSB) – contribution 2) – (solid), and parameters of the kernel – contribution 3) – (dotted). d) Relative importance of the parameters to the contribution 3): a (dotted), d (dashed), and Δz (solid).

tions are plotted in Figure 10c. It is not surprising that in this case contribution 1) is the largest one due to the 15% error in the measurement of K (the calibration constant). The error in the kernel – contribution 3) – is negligible, while contribution 2) – using a filtered kernel – gives a constant error of about 3.5% of the peak value, as compared to the 1% LSB error (relative to its maximum) in the input data. We recall that the LSB error has a strong short wavelength component that has no physical meaning, therefore it is eliminated or reduced as much as possible.

For the current density the situation is quite different. Figures 11 a and b show the inverted current density. The singularity of the kernel makes mandatory to filter up to $\lambda = 4\,\Delta z$, and still short wavelength perturbations are present. In view of this result it is interesting to consider other filters than the explicit one. Error contributions, Fig. 11 c, show that the filtered LSB error is about 4% of the peak value, while the input data exhibit a 1% LSB error. Again the error magnification of the shortest wavelength component is greatly increased notwithstanding the filtering procedure. Contribution 1) reaches a maximum value of the same order as contribution 2), while contribution 3) is the largest one in this case. The influence of each parameter in the last contribution is plotted in Figure 11 d. The larger error in a is almost compensated by the larger sensitivity of the kernel to d, while the influence of Δz can be neglected in this case. The total error in the maximum of the peak is almost 10%, while the largest error occurs at the trailing part of the signal – up to 20% of the peak value –, that is acceptable as compared with the 10% error in a and 5% in A, together with other minor contributions.

With few data points the method also worked well. From an interferogram registered in a film, the fringe

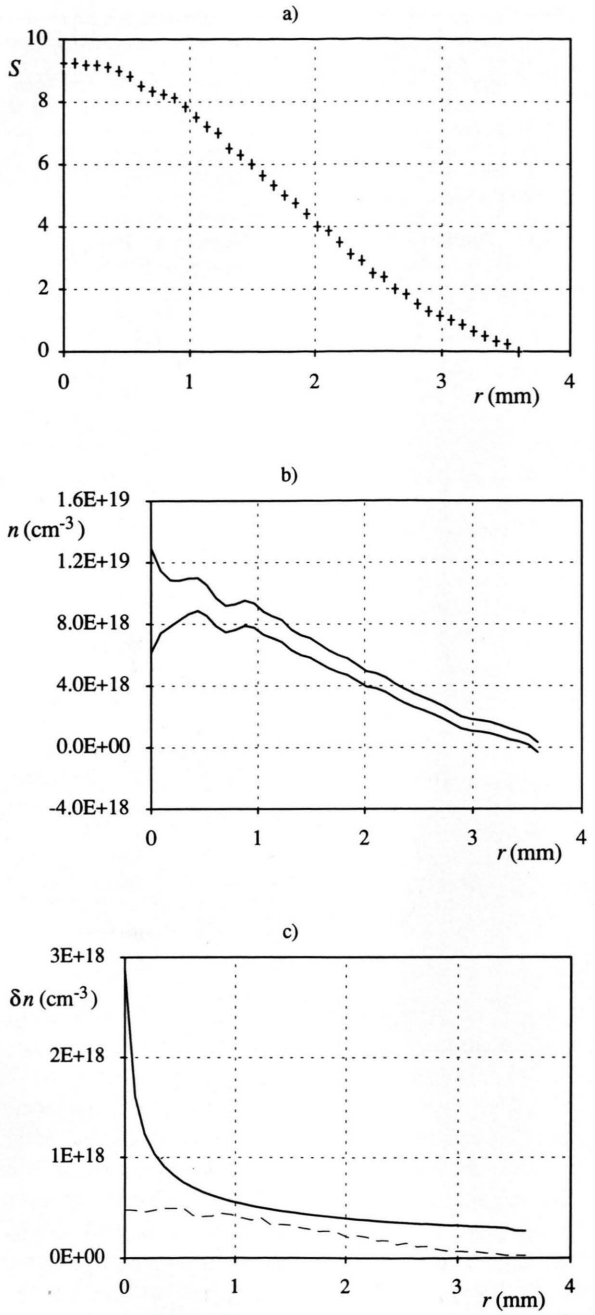

Fig. 12. a) Fringe displacement, and b) its inversion with the error band obtained from an interferogram in a PF discharge. c) Error contributions: scaling factors – contribution 1) – (dashed), and error in the input data – contribution 2) – (solid).

displacement was obtained after capturing the image with a CCD camera, and a fringe analysis was performed. In Fig. 12a the fringe displacement and its inversion is given for $N=41$ and $R=3.6$ mm ($\pm 5\%$). The fringe displacement was measured with $\delta S=0.25$. This error is greatly amplified in the axis of the interferogram, reaching a 30% error. For other points the total error is about 10% as compared to the 5% error in R and several percent error in the fringe displacement.

6. Conclusions

The resolution of first class Volterra equations has the inconvenient of error magnification. This is inherent to the problem and does not depend on the numerical method. Fortunately, only the shortest wavelength perturbations suffer from this illness, that usually is far from any significant physical wavelength and in most cases can be removed or filtered without distorting the physical sense of the integral. The problem is worst when the kernel has a singularity as in the case of the magnetic probe problem. Not only the amplification factor is higher, also a spurious wavelength ($\lambda \approx a$) may be included in the results. While designing the probe it is important to keep this fact in mind.

Using direct methods the evaluation of the error propagation can be performed during the inversion. The derivatives of the resolvent kernel are performed as a difference instead of using the analytical ones (that can be easily calculated), in order to minimize the computer time. If the parameters are fixed, the resolvent kernel together with their derivatives can be evaluated in advance and stored, to minimize the computational inversion time. A full inversion with 1,000 data points requires less than 1 minute in a PC, while having the kernel stored the inversion time plus the error calculations takes few seconds.

The influence in the solution of the errors in the parameters can be inferred by plotting the derivatives of the resolvent kernel. Also the relative importance of the different contributions can be put into evidence in advance, helping in the design and giving hints on the accuracy of the measurement of the parameters.

For signals with a few to several thousands data points, the Matrix method in conjunction with an adequate filter is a good compromise between accuracy and computational speed. Also, it provides a simple way to estimate the errors (using error propagation).

[1] J. Mather, Dense Plasma Focus, in: Plasma Physics, vol. 9b (R. Lovberg and H. Griem, eds.), Academic Press, New York 1971, p. 187.
[2] R. Landeburg and D. Bershader, Interferometry, in: Physical Measurements in Gas Dynamics and Combustion, vol. 9, High Speed Aerodynamics and Jet Propulsion, Princeton University Press, Princeton, New Jersey 1954, p. 47.
[3] P. Morgan, Optical refractivities studies of plasma focus, Ph.D. Thesis, University of London 1974.
[4] H. Bruzzone, C. Moreno, and H. Kelly, Meas. Sci. Technol. **2,** 1195 (1991).
[5] J. H. Malberg, Rev. Sci. Instrum. **35,** 1622 (1964).
[6] L. Bilbao, H. Bruzzone, H. Kelly, and M. Esper, IEEE Trans. Plasma Sci. **13,** 202 (1985).
[7] P. Linz, Analytical and Numerical Methods for Volterra Equations, SIAM Studies in Applied Mathematics (John Nohel, ed.), Siam, Philadelphia 1985.
[8] J. Hadamard, Bull. Princeton University **13,** 82 (1904). See also P. Garabedian, in: Partial Differential Equations, Wiley, New York 1964, p. 109.
[9] F. Weyl, Analysis of Optical Methods, in: Physical Measurements in Gas Dynamics and Combustion, vol. 9, High Speed Aerodynamics and Jet Propulsion, Princeton University Press, Princeton, New Jersey 1954, p. 15.
[10] C. Fleurier and J. Chapelle, Comput. Phys. Commun. **7,** 200 (1974).
[11] K. Bockasten, J. Opt. Soc. Amer. **51,** 943 (1961).
[12] G. Pretzler, H. Jäger, T. Neger, H. Philipp, and J. Woisetschläger, Z. Naturforsch. **47a,** 955 (1992).
[13] Pinhas Alpert, Journal of Computational Physics **44,** 212 (1981).

Verantwortlich für den Inhalt: A. KLEMM
Satz und Druck: Konrad Triltsch, Würzburg